Supporting Information Appendix

Materials and Methods

Confocal reflectance microscopy (CRM) analysis of collagen microstructure

To visualize the microarchitecture of collagen scaffolds, confocal reflectance imaging was performed using a Zeiss 710 confocal microscope on a Zeiss Axio Observer Z1 inverted stand with a 40x water immersion objective. Scaffolds were briefly-fixed by 4% paraformaldehyde (PFA) and then illuminated with a low intensity of 488nm laser split through an 80/20 dichroic beam splitter, and the backscatter light reflected from collagen fibers was collected by a photomultiplier tube. Z-stack images were captured from 5 - 6 random areas per sample with 2 μm intervals and for a total number of 4 - 5 samples.

Scanning electron microscopy (SEM) imaging

ASC-embedded collagen scaffolds were fixed with 2.5% glutaraldehyde in 0.05M cacodylate buffer. The scaffolds were sequentially dehydrated by a series of ethanol solutions (25%, 50%, 75%, 95%, and 100%) and dried by a treatment with hexamethyldisilazane (Electron Microscopy Sciences). Then, the samples were mounted on the conductive carbon adhesive tab (Electron Microscopy Sciences) and coated with gold/palladium alloy using a sputter coater (Denton Vacuum, Desk II). Images were captured with a Tescan, Mira3 LM scanning electron microscope.

Image analysis of collagen scaffold microarchitecture

The mean pore and fiber diameter of the differently fabricated collagen scaffolds were analyzed using a custom-built automated algorithm as described previously[1]. Briefly, SEM images were

transformed to black and white binary images using a constant threshold. Subsequently, the mean pore diameter was obtained by generating circular disks with varying diameters to cover the pore area in each image and calculate the mean diameter of the disks necessary to cover 50% of the pore area in the image. An autocorrelation method was utilized to evaluate the diameter of heterogeneously-oriented collagen fibers. Collagen fiber linearity was calculated by the ratio of the shortest length over the longest length of each individual fiber based on SEM images. 4 images were analyzed per sample.

Image analysis of collagen fiber alignment

To analyze collagen fiber alignment in the 3D cultures, we have used an analytical model that recognizes fibers in radial and tangential alignment of a defined circle in 3D imaging data sets. To this end, we have embedded ASC spheroids generated as previously described[2] into cold-cast collagen scaffolds, and analyzed individual cells 180 μm above the spheroid core where cells had individually migrated into the matrix. In order to analyze the collagen fibril alignment, linear texture features of images were extracted using a Gabor analysis using a 2D kernel G (k_x, k_y) computed as follows:

$$G(k_x, k_y) = \frac{-(k_x{}^2 + k_y{}^2)}{2\sigma^2} \cos\left(\frac{2\pi k_y}{\gamma}\right).$$

Here σ and γ are related to the length and width of the features, respectively. The images acquired had a pixel resolution of 0.865 μm. For analysis, we used a 19x19 pixel kernel with σ = 4.33 μm and γ = 6.92 μm. At each pixel, the filter was rotated circumferentially or radially with respect to the center of the spheroid, the kernel was multiplied by image fluctuations and summed, and the result was added to the red or green channels respectively in the analysis

images. To determine the radial/circumferential alignment, the total pixel intensities of the two channels were summed and divided. All image analysis was performed using the IDL data visualization language (L3 Harris Geospatial).

Dynamic Mechanical Thermal Analysis (DMTA) of 3D collagen scaffolds

The compressive moduli of collagen scaffolds were measured by dynamic mechanical thermal analysis (DMTA) as previously described[3]. The measurement was performed with a standard submersion-compression clamp configuration at room temperature (25^{o}C) while the samples were kept hydrated in phosphate-buffered saline (PBS). Given 10% pre-strain (0.001N), which prevented slippage of the sample, the compressive tests were run on each sample under the controlled force up to 0.1N. The rate of force application was kept constant at 0.01 N/min in all tests. The force F (force sensitivity of 0.001 N) and thickness L (distance resolution of 0.05 μm) were measured simultaneously and converted into stress-strain plots as follows: strain, $\varepsilon = (L_o - L)/L_o$ (where L_o is the initial thickness and L the thickness of compressed sample) and stress, $\sigma = F/A_o$ (where F is the applied force, and A_o the initial surface area). Young's modulus, E, was the slope of the stress-strain curve, $\sigma = E\,\varepsilon$ in the low-strain (15 - 23 %) elastic regime and the mean of Young's modulus [E] was obtained from 4 different samples per condition.

Atomic Force Microscopy (AFM) analysis of 3D collagen scaffolds

The local compressive moduli of the different collagen scaffolds were assessed by AFM using a MFP-3D-AFM scanning probe microscope (Asylum Research) mounted onto an Olympus IX-71 inverted optical microscope. AFM measurements were performed in contact mode while the scaffolds were submerged in PBS. Twenty randomly selected regions of each scaffold were

probed using a 5 μm diameter borosilicate glass sphere attached to a silicon nitride cantilever (Novascan Tech). The thermal calibration was performed prior to each measurement to determine the nominal spring constant k (~ 0.06 N/m) of the cantilever. To record full force-indentation loading curves, the scaffolds were being indented (V ≤ 100 nm/s) until the applied force reached a pre-determined force limit (~ 20 nN). For analysis, the curves were fitted to the Hertz spherical indentation model;

$$F = \frac{4}{3} E \sqrt{R} \delta^{\frac{3}{2}}$$

where F is applied force, R is the radius of the glass sphere (R ~ 5 μm), δ is indentation of the scaffolds, and E is Young's modulus of the scaffolds. Utilizing IGOR PRO software (WaveMetrics), Young's moduli (E) were calculated based on the resulting fit coefficients as the Poisson's ratio was set to 0.5.

Analysis of fibronectin conformation in 3D collagen scaffolds via FRET

Fibronectin (Fn) conformational changes in 3D collagen scaffolds were analyzed via Förster Resonance Energy Transfer (FRET) imaging technique as previously described[4,5]. ASCs in the scaffolds were pre-cultured for 3 days to allow ASCs to deposit native Fn matrices. 50 μg/mL of human plasma Fn consisting of 10% FRET-labeled and 90% unlabeled-Fn was supplemented and the cultures were maintained for 1, 2, or 3 additional days. Subsequently, collagen scaffolds were fixed and then imaged using a Zeiss 710 confocal microscope with a 40x water immersion objective at 2 μm intervals. FRET-labeled Fn in the scaffolds was excited by a low intensity (10%) of 488 nm laser, and signals from the donor (514-526 nm) and acceptor (566-578 nm) channels were collected. Positive signals were selected based on strictly-determined threshold intensity, and FRET intensity ratio (acceptor to donor intensity) was calculated using MATLAB

(MathWorks, Inc.)[4,5]. The threshold intensity was obtained by averaging the highest signals from cell- and Fn-free regions in each Z-stack. Additionally, we confirmed that there was no difference in FRET intensity ratio of cold- vs. warm-cast scaffolds when no cells were present. 5 Z-stacks per sample, and three samples per condition were analyzed to determine the mean and standard deviation of the FRET intensities, and the histogram plots were generated to indicate FRET intensity at each representative location.

Immunofluorescence

Samples were briefly fixed with 4% PFA and washed in PBS. Subsequently, the samples were permeabilized in 0.05% Triton X-100 (VWR) in PBS (PBS-X), blocked in 1% BSA (Fisher Scientific) in PBS, and incubated with primary antibodies against α-SMA (Abcam), Desmin (Abcam), p-MLC (phospho S20) (Abcam), Fn (Invitrogen), YAP (Santa Cruz Biotechnology) in 0.05% PBS-X overnight at 4°C. AlexaFluor 488 or 647 conjugated secondary antibody was used to label α-SMA, desmin, Fn, YAP; Alexa Fluor 568 Phalloidin for cytoskeleton; and counterstained with 4',6-diamidino-2-phenylindole (DAPI). For image analysis of YAP, 4 representative images were captured per sample for a total of 3 samples using a Zeiss i880 microscope with a 32x water immersion objective. For all other samples, 10 fields of view per sample for a total of 3 samples were randomly selected and imaged with a Zeiss 710 confocal microscope with a 25×/0.8 water immersion objective. The average positive pixel intensity or number of positive cells was obtained based on strict threshold intensity using Image J (NIH) and then normalized to cell number.

Analysis of pro-angiogenic factor secretion

ASCs were cultured in cold- or warm-cast scaffolds with their growth media for 6 days, and the media was replaced with DMEM/F12 (Gibco) with 1% FBS, and 1% penicillin/streptomycin. After 24 hours, conditioned media were collected to analyze the levels of vascular endothelial cell growth factor (VEGF) and interleukin-8 (IL-8) by VEGF and IL-8 ELISA duo set (R&D), respectively. DNA was extracted from the cells lysed in Caron's buffer (25mM Tris-HCl, 0.4M NaCl, 0.5% SDS), and measured by QuantiFluor® dsDNA System (Promega) following the manufacturer's protocols to normalize VEGF and IL-8 levels. Each experiment with 3 samples per condition was performed in triplicate.

Endothelial cell sprouting assay

First, ASCs were pre-cultured in cold- vs. warm-cast scaffolds for 6 days. Then, HUVECs were seeded on top of the scaffolds at a density of 300 cells/mm^2 and incubated for 1 hour. Once HUVECs were adhered, invasion media containing HUVEC-GM, 1% [v/v] L-ascorbic acid (50 μg/mL; Acros Organics, Morris Plains, NJ), and 0.16% [v/v] tetradecanoyl phorbol acetate (50 ng/mL; Cell Signaling Technology, Inc., Danvers, MA) were added to the cells and changed every other day for up to 4 days. For VEGF and IL-8 inhibition, HUVECs were cultured in the invasion media supplemented with 1 μg/ml of VEGF and/or IL-8 neutralizing antibodies (both from R&D) for 4 days. HUVEC sprouting was assessed by confocal image analysis after immunofluorescence staining for CD31 (Sigma-Aldrich). 5 to 6 Z-stack images per sample for a total of 3 samples were obtained by Zeiss 710 confocal microscope with a 25×/0.8 water immersion objective at 5 μm intervals. HUVEC sprouts exceeding a length of 15 μm were manually counted and the average number of sprouts per condition was obtained from the counts of 3 samples. Each experiment was performed in triplicate.

Pharmacological inhibition of cell contractility

To assess the effect of cell contractility, ASCs in cold or warm-cast scaffolds were cultured with Y27632 Rho/ROCK inhibitor (Tocris), which blocks Rho-mediated cell contraction[6]. 10 μM of Y27632 in DMEM/F12 with 1% FBS and 1% antibiotics were freshly prepared and added to the cells every other day for up to 6 days. The levels of pro-angiogenic factors secreted by ASCs and HUVEC sprouting were assessed as described above. Blebbistatin experiments were performed by adding 20uM blebbistain (Krackeler Scientific, 45-B0560-5MG) to the culture medium every 2 days. After 3 days of treatment, samples were fixed, stained for F-actin and α-SMA and imaged as stated above.

References

1 Franke, K., Sapudom, J., Kalbitzer, L., Anderegg, U. & Pompe, T. Topologically defined composites of collagen types I and V as in vitro cell culture scaffolds. *Acta Biomater* **10**, 2693-2702, doi:10.1016/j.actbio.2014.02.036 (2014).

2 Vidavsky, N. *et al.* Studying biomineralization pathways in a 3D culture model of breast cancer microcalcifications. *Biomaterials* **179**, 71-82, doi:10.1016/j.biomaterials.2018.06.030 (2018).

3 Chandler, E. M. *et al.* Implanted adipose progenitor cells as physicochemical regulators of breast cancer. *Proc Natl Acad Sci U S A* **109**, 9786-9791, doi:10.1073/pnas.1121160109 (2012).

4 Smith, M. L. *et al.* Force-induced unfolding of fibronectin in the extracellular matrix of living cells. *PLoS biology* **5**, e268, doi:10.1371/journal.pbio.0050268 (2007).

5 Wang, K. *et al.* Breast cancer cells alter the dynamics of stromal fibronectin-collagen interactions. *Matrix Biol* **60-61**, 86-95, doi:10.1016/j.matbio.2016.08.001 (2017).

6 Seo, B. R. *et al.* Obesity-dependent changes in interstitial ECM mechanics promote breast tumorigenesis. *Sci Transl Med* **7**, 301ra130, doi:10.1126/scitranslmed.3010467 (2015).

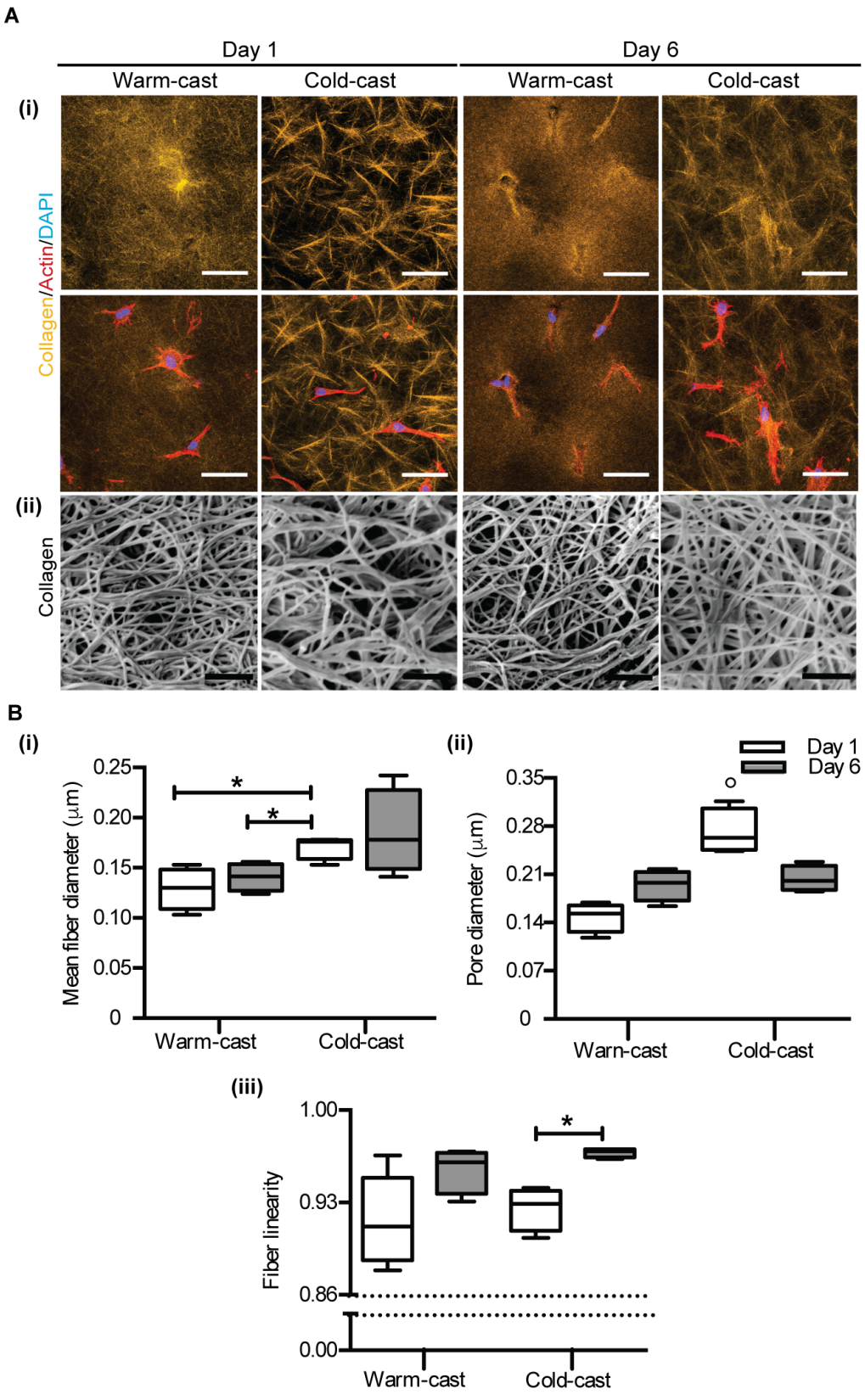
A
Day 1
Day 6
Warm-cast
Cold-cast
Warm-cast
Cold-cast
(i)
Collagen/Actin/DAPI
(ii)
Collagen
B
(i)
Mean fiber diameter (μm)
0.25
0.20
0.15
0.10
0.05
0
*
*
Warm-cast
Cold-cast
(ii)
Day 1
Day 6
Pore diameter (μm)
0.35
0.28
0.21
0.14
0.07
0
Warn-cast
Cold-cast
(iii)
Fiber linearity
1.00
0.93
0.86
0.00
*
Warm-cast
Cold-cast

Fig. S1 Collagen microarchitecture in the presence of ASCs.
(A) (i) Representative CRM images of collagen scaffolds with ASCs on day 1 and day 6 of culture. Collagen (yellow), cytoskeleton (red), cell nuclei (blue) (Scale bars = 50 μm). (ii) SEM images of collagen microarchitecture of ASC-seeded scaffolds on day 1 and 6 of culture. (Scale bars =1 μm). **(B)** SEM image-based analysis of cell-mediated changes of collagen (i) fiber diameter, (ii) pore diameter and (iii) fiber linearity on day 1 and day 6. * and ○ indicate $p < 0.05$ between two and all other conditions, respectively.

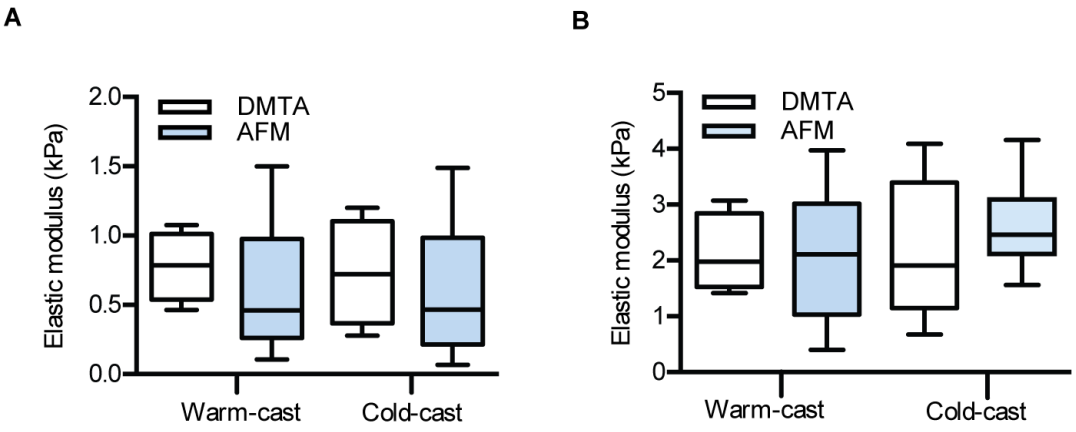

Fig. S2 Compressive moduli of collagen scaffolds with and without ASCs. (A) Compressive elastic modulus (15% - 23%) of cell-free collagen scaffolds at the bulk and local scale as determined via dynamic mechanical analysis (DMTA) and atomic force microscopy (AFM), respectively. **(B)** Compressive elastic moduli of ASC-seeded collagen scaffolds as assessed via DMTA and AFM after 6 days of culture.

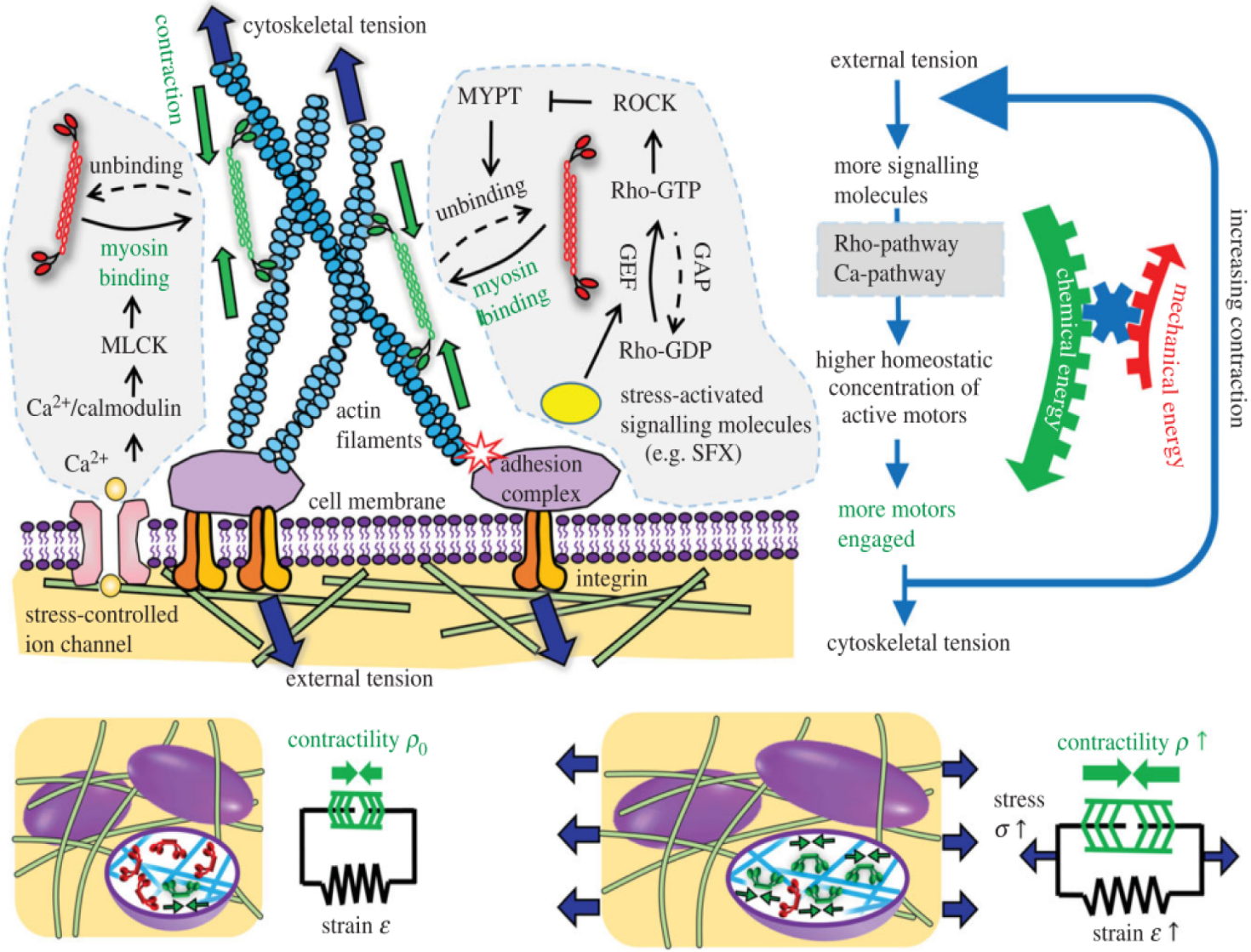
cytoskeletal tension
contraction
unbinding
myosin binding
MLCK
Ca2+/calmodulin
Ca2+
MYPT
ROCK
unbinding
Rho-GTP
myosin binding
GEF
GAP
Rho-GDP
stress-activated signalling molecules (e.g. SFX)
actin filaments
adhesion complex
cell membrane
integrin
stress-controlled ion channel
external tension
external tension
more signalling molecules
Rho-pathway Ca-pathway
higher homeostatic concentration of active motors
more motors engaged
cytoskeletal tension
chemical energy
mechanical energy
increasing contraction
contractility ρ_0
strain ε
contractility $\rho\uparrow$
stress $\sigma\uparrow$
strain $\varepsilon\uparrow$

Fig. S3 Schematic representation of the cell contractility model. The Rho-ROCK and Ca-pathways are regulated by stress signals on the cell membrane. When a cell is under tension, a series of biochemical processes is activated, and ultimately, more myosin motors switch from an inactive state (red) to an active state (green), which promotes their binding to the cytoskeleton and creates more force dipoles inside the cell. Collectively, these force dipoles lead to contraction of the ECM.

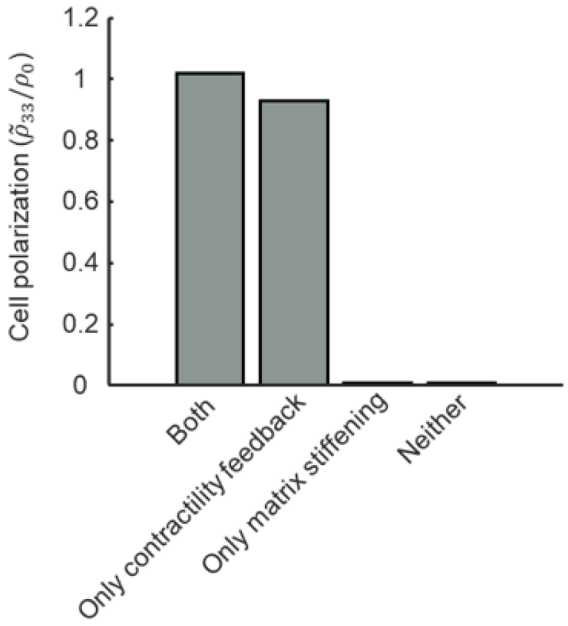

Fig. S4 Feedback relationship between contractility feedback, matrix strain stiffening, and polarization of cell contractility. Impact of the contractility feedback and the matrix strain stiffening on the polarization of cell contractility as determined by computational simulation. Four simulations are shown: both are present, only cell contractility feedback is present, only matrix strain-stiffening is present, and neither is present.

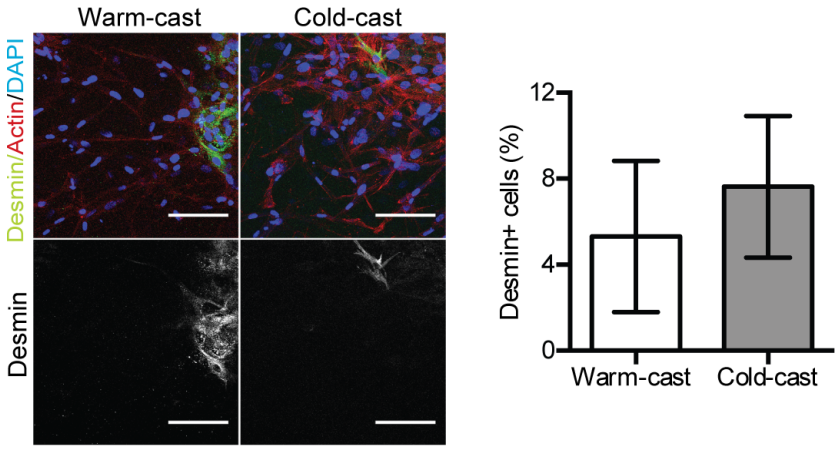

Fig. S5 Analysis of desmin positive ASCs in cold- vs. warm-cast scaffolds. Confocal micrographs of cells stained for desmin (green), F-actin (red) and nuclei (blue) and corresponding quantification of desmin levels via image analysis.

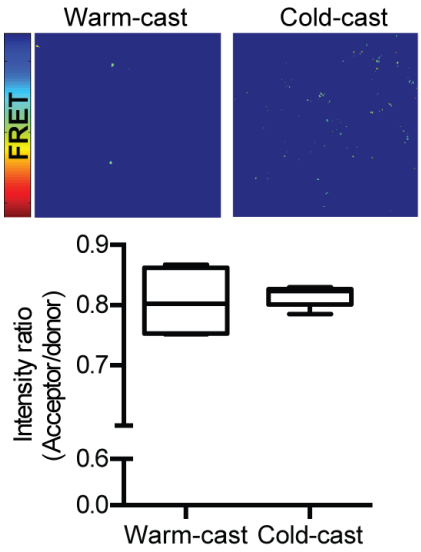

Fig. S6 FRET analysis of fibronectin (Fn) conformation in cell-free collagen scaffolds. Analysis of FRET intensity between cold- and warm-cast scaffolds in the absence of ASCs 72 hours after incorporation of FRET-labeled Fn (Scale bar = 50 μm).

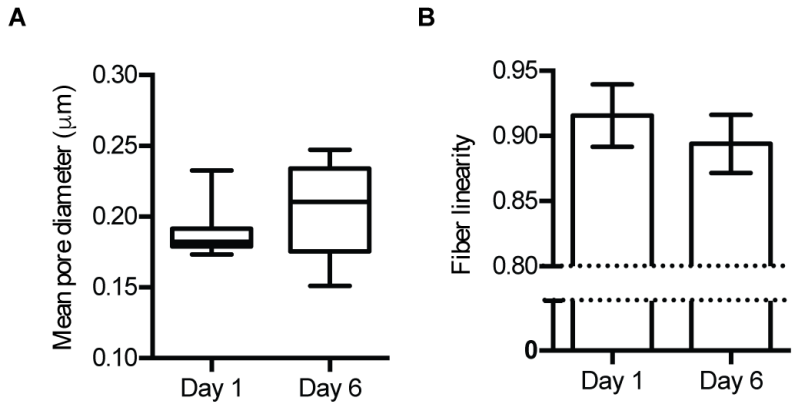

Fig. S7 Effect of media incubation on the microarchitecture of cell-free, cold-cast collagen scaffolds. (A) Pore size and **(B)** fiber linearity of cell-free, cold-cast collagen scaffolds after 1 and 6 days of incubation with cell culture media as determined by SEM-based image analysis.

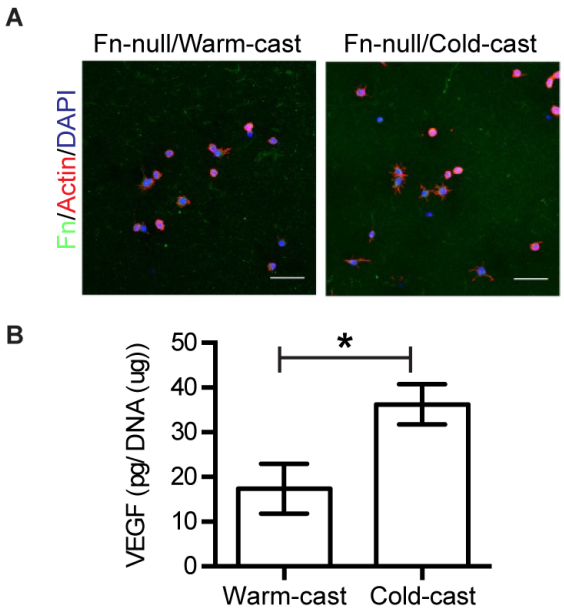

Fig. S8 VEGF secretion of Fn-null MEFs in warm- and cold-cast collagen scaffolds. **(A)** IF images of Fn matrix (green) and Fn-null MEFs (red: actin, blue: nuclei) in warm- and cold-cast scaffolds. **(B)** Quantification of VEGF secretion by Fn-null MEFs in cold- vs. warm-cast collagen scaffolds as determined by ELISA and normalized to DNA content (Scale bar = 50 μm).

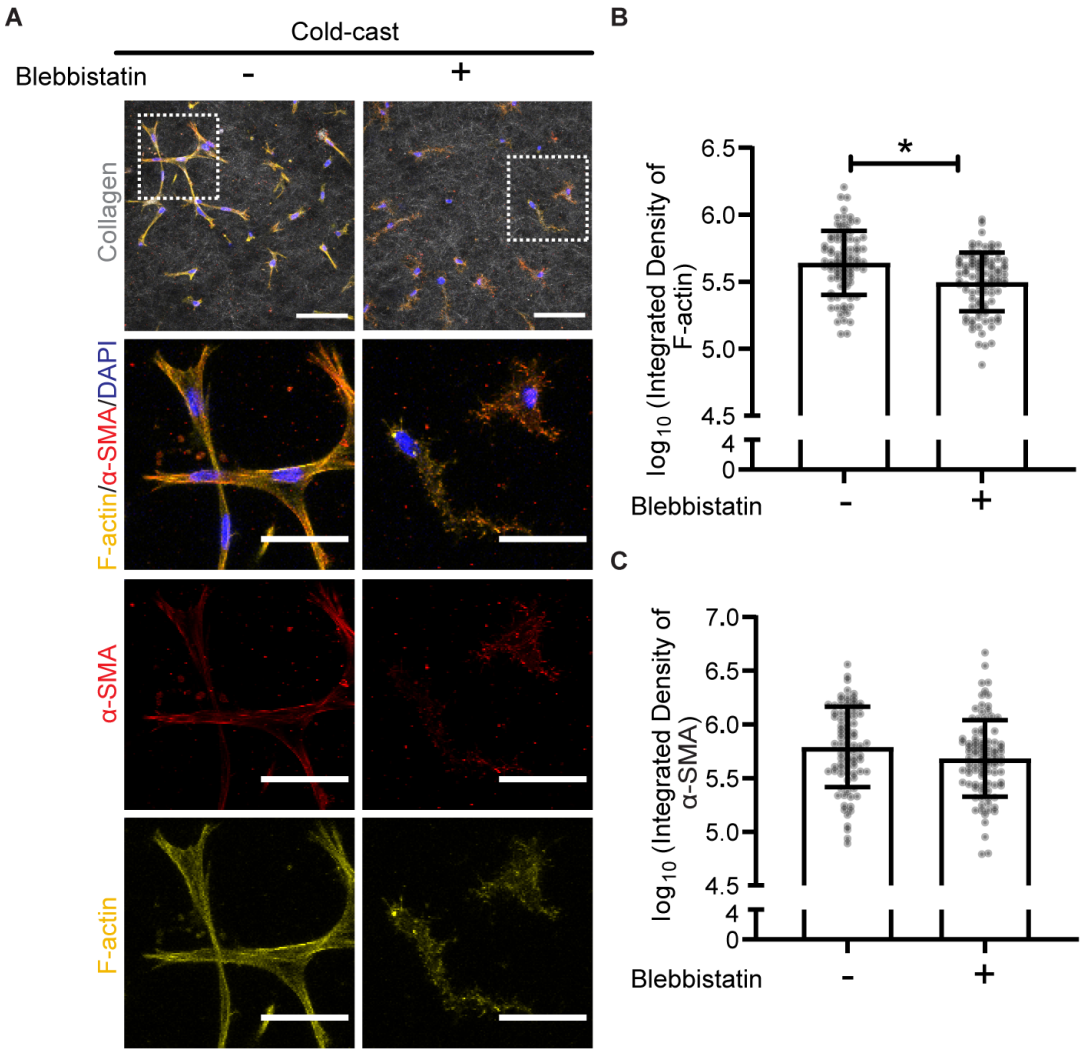

Fig. S9 Effect of blebbistatin on F-actin and α-SMA fiber assembly of ASCs in cold-cast collagen scaffolds. (A) CRM and IF images of collagen matrix (white) and ASCs (red: α-SMA, yellow: actin, blue: nuclei) in cold-cast scaffolds with and without blebbistatin treatment. **(B & C)** Quantification of F-actin and α-SMA intensity in cold-cast collagen scaffolds in the absence or presence of blebbistatin treatment as determined by IF image analysis (Scale bar = 50 μm). The data were log-transformed and assessed with unpaired t-test for statistical analysis. * indicates $p < 0.05$.

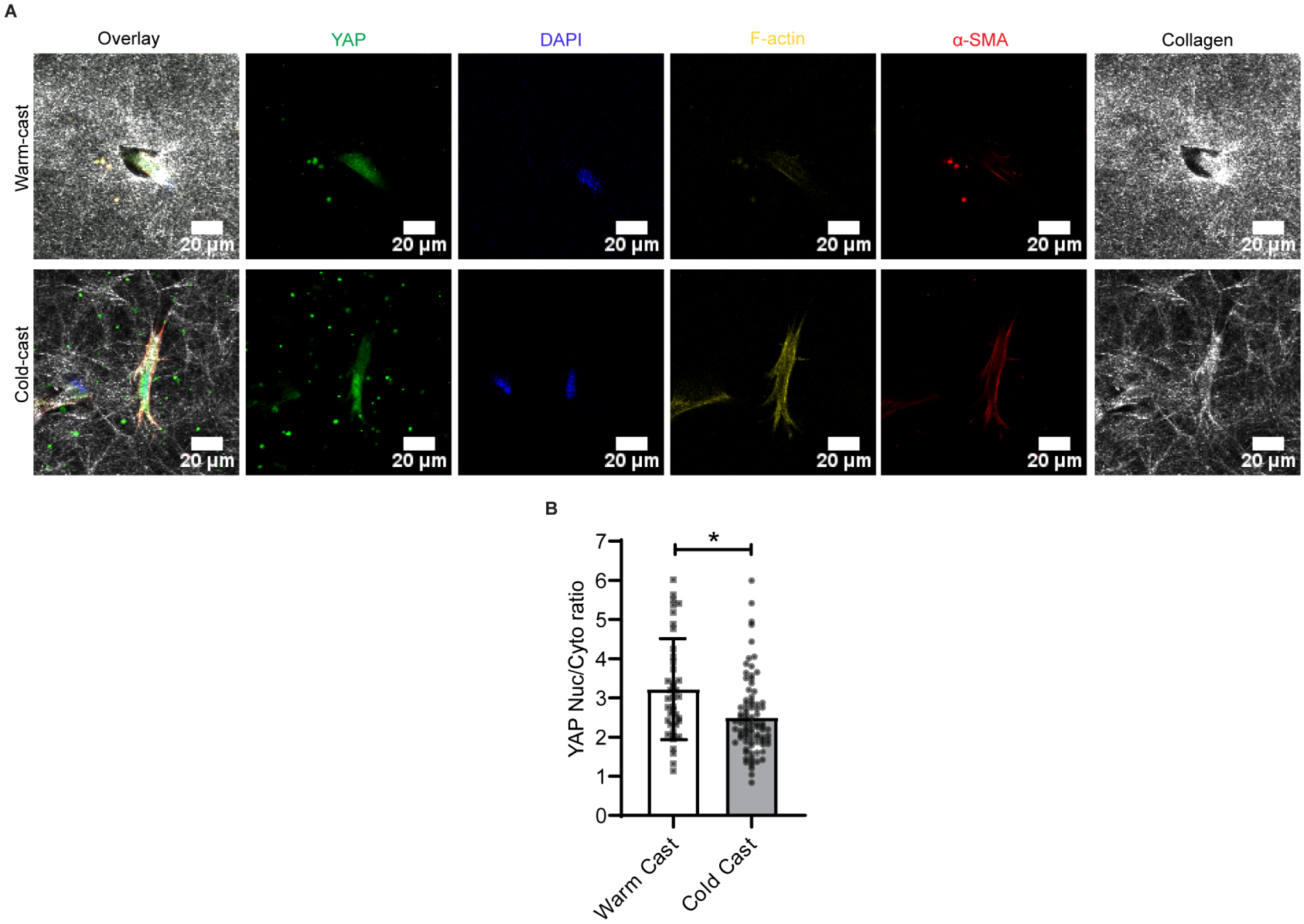
A
Overlay
YAP
DAPI
F-actin
α-SMA
Collagen
Warm-cast
Cold-cast
20 μm
B
YAP Nuc/Cyto ratio
0
1
2
3
4
5
6
7
*
Warm Cast
Cold Cast

Fig. S10 Nuclear translocation of YAP in warm- and cold-cast collagen scaffolds. **(A)** CRM and IF images of collagen matrix (white) and ASCs (green: YAP, red: α-SMA, yellow: actin, blue: nuclei) in warm- and cold-cast scaffolds. **(B)** Ratio of nucleus-specific YAP relative to cytoplasmic YAP intensity as determined by IF image analysis (Scale bar = 20 μm).

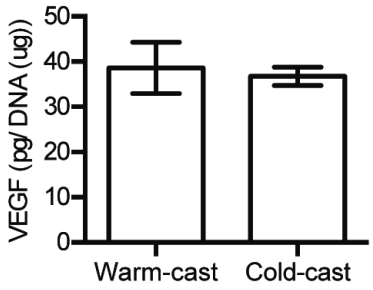

Fig. S11 Effect of collagen microarchitecture on VEGF ECM sequestration. Quantification of matrix-bound VEGF from cold- and warm-cast scaffolds as determined by ELISA of whole culture lysates after culturing ASCs in the scaffolds for 6 days.